Published in final edited form as:

Biochem J. 2020 October 16; 477(19): 3851–3866. doi:10.1042/BCJ20190776.

ShNPSN11, a vesicle-transport-related gene, confers disease resistance in tomato to *Oidium neolycopersici*

Qinggui Lian[1,*], **Yanan Meng**[1,2,*], **Xinbei Zhao**[1], **Yuanliu Xu**[1], **Yang Wang**[1], **Brad Day**[3,4], **Qing Ma**[1]

[1]College of Plant Protection, Northwest A&F University, Yangling, Shaanxi 712100, China;

[2]College of Life Sciences, Northwest University, Xi'an, Shaanxi 710069, China;

[3]Department of Plant, Soil and Microbial Sciences, Michigan State University, East Lansing, MI 48824, U.S.A.;

[4]Plant Resilience Institute, Michigan State University, East Lansing, MI 48824, U.S.A.

Abstract

Tomato powdery mildew, caused by *Oidium neolycopersici*, is a fungal disease that results in severe yield loss in infected plants. Herein, we describe the function of a class of proteins, soluble N-ethylmaleimide-sensitive factor attachment protein receptors (SNAREs), which play a role in vesicle transport during defense signaling. To date, there have been no reports describing the function of tomato SNAREs during resistance signaling to powdery mildew. Using a combination of classical plant pathology-, genetics-, and cell biology-based approaches, we evaluate the role of *ShNPSN11* in resistance to the powdery mildew pathogen *O. neolycopersici*. Quantitative RT-PCR analysis of tomato *SNAREs* revealed that *ShNPSN11* mRNA accumulation in disease-resistant varieties was significantly increased following pathogen, compared with susceptible varieties, suggesting a role during induced defense signaling. Using *in planta* subcellular localization, we demonstrate that ShNPSN11 was primarily localized at the plasma membrane, consistent with the localization of SNARE proteins and their role in defense signaling and trafficking. Silencing of *ShNPSN11* resulted in increased susceptibility to *O. neolycopersici*, with pathogen-induced levels of H_2O_2 and cell death elicitation in *ShNPSN11*-silenced lines showing a marked reduction. Transient expression of *ShNPSN11* did not result in the induction of a hypersensitive cell death response or suppress cell death induced by BAX. Taken together, these data demonstrate that *ShNPSNl11* plays an important role in defense activation and host resistance to *O. neolycopersici* in tomato LA1777.

Correspondence: Brad Day (bday@msu.edu) or Qing Ma (maqing@nwsuaf.edu.cn).
*These authors contributed equally to this work.

Author Contributions

Q.L., Y.M., X.Z., and Y.X. performed the experiments. Q.L., Y.M., X.Z., Y.X., B.D., Y.W., and Q.M. analyzed the data. Q.L., B.D., and Q.M wrote the manuscript. All authors have read and approved the final manuscript.

Competing Interests

The authors declare that there are no competing interests associated with the manuscript.

Introduction

Oidium neolycopersici is a widely distributed and destructive fungal pathogen of tomato (*Solanum lycopersicum* L.) that elicits powdery mildew disease, a pervasive disease of numerous plants species, globally. The disease is easily identifiable, with the appearance of characteristic white powdery spots on the leaves and stems of young, developing, plants [1]. As the infection and disease progresses, infected zones enlarge and the pathogen reproduces through the production of asexual sporulation, following which, the infection spreads throughout the plant. Early research describing possible mechanisms of infection, as well as modes of host resistance, primarily utilized wild relatives of tomato, primarily focusing on leveraging wild germplasm as potential sources of resistance [2]. More recently, research in this area has focused on the identification and characterization of resistance alleles, including those associated with resistance to a range of downy mildew pathogens. For example, studies investigating the function of the MLO1 locus from tomato (i.e. SlMLO1) have shown that a deletion of a 19 bp segment — yielding an allele referred to as ol-2 — confers resistance in tomato to *On*-lz [3]. Interestingly, this mechanism is similar to that of the MLO gene in barley [4].

Penetration resistance, a key feature of host immunity to fungi, has been widely characterized as a rapid and highly effective mechanism of defense signaling in response to fungal pathogens [5]. In short, this mechanism of resistance is associated with the rapid activation of a papilla response in the host, whereby a dome-shaped cell wall apposition is deposited by the epidermal cells between the cell wall and plasma membrane (PM) at the site of penetration. In the model non-host interaction system — Arabidopsis and *Blumeria graminis* f. sp. *hordei* [6] — non-host resistance has been demonstrated to be mediated by the action of the syntaxin PEN1 and its interacting soluble N-ethylmaleimide-sensitive factor attachment protein receptors (SNAREs) proteins, SNAP33 and VAMP721/2 [7]. Similarly, in *Puccinia striiformis* f. sp. *tritici (Pst)*, a biotrophic fungal pathogen of wheat, previous research reported that NPSN11, a novel wheat SNAREs, is required for vesicle-mediated resistance to stripe rust [8]. In total, a role for SNARE proteins as key components of host defense signaling against fungal pathogen invasion is starting to emerge.

SNARE signaling complexes are comprised of four key components: A single vesicle membrane-anchored SNARE (v-SNARE), which are located on the transport vesicles membrane, and three target membrane-anchored SNAREs (t-SNAREs; e.g. R, Qa, Qb, and Qc domains), located on the target membrane [9–11], which determine the specificity of intracellular fusion processes and signaling. As a family, SNAREs are the primary components of vesicle trafficking processes in eukaryotic cells [12], a function which is mediated by their ability to bring recruit cell membranes within close proximity of one another. SNARE proteins have been extensively characterized for their roles in development [13], response to abiotic stress [14], as well as for their involvement in defense signaling following pathogen infection [15]. Indeed, and as noted above, a role for SNARE proteins is emerging during resistance signaling to a range of plant pathogens [16]. Further examples also include *HvSNAP34* [17], which is required for defense-induced callose deposition, as well as *NbSYP132* from *Nicotiana tabacum*, which mediates the secretion of pathogenesis-related protein-1 (PR-1) following bacterial pathogen infection [18]. Additionally, using

loss-of-function approaches, recent work has also shown that the Golgi-associated SNARE *AtMEMB12* is targeted by miR393b* and promotes secretion of PR1 in Arabidopsis [19]. In contrast with roles in defense signaling, the SNAREs protein Syp71 is an essential host factor for successful *Turnip Mosaic Virus* infection by mediating the fusion of the virus-induced vesicles with chloroplasts during turnip mosaic virus infection [20].

While the function and activity of numerous SNAREs have been defined in vesicle transport processes [9,21–24], their role in the signaling of resistance during infection of tomato by a downy mildew pathogen is unknown. In the current study, we describe a role for *ShNPSN11* in defense signaling following infection of tomato with the downy mildew pathogen O. *neolycopersici*. Analysis of the expression of tomato *SNAREs* mRNAs were analyzed following *On*-lz infection, leading to the identification of one highly induced mRNA, *ShNPSN11*, which was selected for further analysis. Cloning, sequencing and *in silico* characterization of *ShNPSN11* confirmed similarity to known SNARE genes from tomato and other plant species. The transcriptional activity of *ShNPSN11* in response to *On*-lz was characterized using qRT-PCR, and further loss-of-function analyses using virus-induced gene silencing (VIGS) assay with *tobacco rattle virus* (TRV1 and TRV2), support a role for NPSN11 in defense signaling following *On*-lz. In total, the work described herein contributes to a growing — yet understudied — body of research describing the function of SNARE-complex signaling during pathogen infection in plants.

Materials and methods

Plant, pathogen growth, and inoculation experiments

Two genotypes of tomato were used in this study: *Solanum habrochaites* LA1777 and Money Maker (MM) (*S. lycopersicum*), both of which were obtained from the Tomato Genetics Resource Center (Department of Plant Sciences, University of California, Davis). *S. habrochaites* LA1777 is resistant to *On*-lz, while Money Maker is highly susceptible to *On*-Lz. For germination and growth, tomato seeds were surface sterilized according to the method of Sun et al. [25] and grown in growth chamber with 16 hours (h) photoperiod (22°C, 80–90% relative humidity).

Nicotiana benthamiana plants were grown in a growth chamber at 20°C under a 16 h light/8 h dark cycle with 60% relative humidity and a light intensity of 120 mmol photons m^{-2} sec^{-1}.

Oidium neolycopersici strain Lanzhou (*On*-Lz) was propagated and preserved according to the method of Sun et al. [26].

Escherichia coli strain DH5α was grown at 37°C on Luria–Bertani (LB) medium containing antibiotics. *Agrobacterium tumefaciens* strain GV3101 harboring binary vector constructs was grown on antibiotic-containing LB media at 28°C.

For pathogen inoculation assays, *On*-Lz was sprayed onto 8-day-old plants with a suspension of ~10^5 spores ml^{-1} according to the method of Zheng et al. [27]. Spore counts

were quantified using a hemocytometer. Inoculated tomato seedling were grown in environmentally controlled growth chambers under the same conditions as described above.

Quantitative RT-PCR (qRT-PCR) analysis

For the evaluation of *SNARE* mRNA accumulation, 2-week-old LA1777 and Money Maker plants were used. Plants were inoculated with a suspension of *On*-lz (~10^5 spores ml^{-1}) or mock-inoculated (water), and samples were collected at 0, 6, 12, 24, 48, 72, 96, and 120 h post inoculation (hpi) from all treatments, flash-frozen in liquid nitrogen, and stored at −80°C. In all cases, treatments were replicated three times with 6 plant seedlings in each replicates.

Total RNA was extracted from the above samples using the BioZOL reagent (Biomiga, Shanghai, China). Complementary DNA (cDNA) synthesis was performed using a PrimeScript™ RT Reagent Kit with gDNA Eraser (Takara Biotechnology Co. Ltd., Dalian, China) according to the manufacturer's instructions. *Arabidopsis thaliana* SNARE-related proteins [28] were used to screen (*in silico*) the gene databases of tomato [29,30]. Using this approach, a total eight genes were selected for use in the current study. DNA primers for quantitative real-time (RT)-PCR (qRT-PCR) (Supplementary Table S1) were designed using Beacon Designer (Premier Biosoft, Palo Alto, U.S.A.). PCR reactions consisted of 10 µl 2× Ultra SYBR Mixture (CWBio, Beijing, China), 40 nM each primer, and 2 µl 1 : 10-diluted template cDNA in a total volume of 20 µl. No template controls were set for each primer pair. qRT-PCR was performed using the Bio-Rad CF X96 System and Opticon Monitor software (Bio-Rad, Hercules, CA, U.S.A.). Cycling parameters were as follows: 95°C for 1 min; 40 cycles at 95°C for 10 s, 60°C for 10 s; and 72°C for 40 s. Finally, dissociation curves were generated by increasing the temperature from 65°C to 95°C. All analyses were repeated in biological triplicate, each repeat of which contained two technical replicates. mRNA expression values were calculated using the $2^{-\Delta\Delta CT}$ method [31] using *GLYCERALDEHYDE-3-PHOSPHATE DEHYDROGENASE* (*SlGAPDH*) as an internal control.

Cloning and sequence analysis of *ShNPSN11*

The open-reading frame of *ShNPSN11* was amplified from cDNA using gene-specific DNA primers: *ShNPSN11*-F (5′-ATGGCGTCGTTGTCTGGCC-3′) and *ShNPSN11*-R (5′-TCAGTAAGGATAAGCAAGTAACCGTC-3′), designed using Primer Premier ver. 6.0 (Palo Alto, CA, U.S.A.) based on the sequence of *ShNPSN11*. The resultant clone was confirmed by DNA sequencing.

The sequence of *ShNPSN11* was analyzed *in silico* using the online BLAST interface, coupled with ORF Finder (NCBI; https://www.ncbi.nlm.nih.gov/orffinder/). The amino acid sequence of *Sh*NPSN11 was analyzed using Prot Param (https://web.expasy.org/protparam/), Uniprot (https://www.uniprot.org/), and ProtComp (http://linux1.softberry.com/berry.phtml?topic=protcomppl&group=programs&subgroup=proloc). Multiple sequence alignments were performed using CLUSTALX2.0 and DNAMAN6.0 (Lynnon BioSoft; https://www.lynnon.com/). A phylogenetic tree was constructed using the neighbor-joining method using MEGA 6.0 (https://www.megasoftware.net/home).

The promoter of *ShNPSN11* ($P_{ShNPSN11}$) (0_to_−3270) was first analyzed by PlantCARE and Softberry. Next, the promoter of *ShNPSN11* was cloned into the expression vector pCAMBIA0390-GUS using the DNA primers $P_{ShNPSN11}$-F (5′-tggctgcaggtcgacggatccCTCATCGGCATGTATATCAGAA-3′) and $P_{ShNPSN11}$-R (5′-tcttagaattcccggggatccTTTAGGACGTTCAGTTTAGGG-3′), and the recombinant vector was transformed into Agrobacterium strain GV3101 for transient expression [32]. Agrobacterium-mediated transient assay was performed on the leaves of 4-week-old *N. benthamiana*, containing four series: wild type (WT), pCAMBIA0390::35S-GUS, pCAMBIA0 390-GUS and pCAMBIA0390:: $P_{ShNPSN11}$-GUS. The *N. benthamiana* for transient expression were cultivated in a 22°C chamber with 16 h light/8 h dark cycle for 2 days before the treatment with 100 μM MeJA, 10 mM SA and water (Control) (Sigma, Shanghai, China), respectively. All treatments were three replicates, each replicate containing three seedlings. At 48 h after treatments, the tobacco leaves were collected for detection of GUS activity. Histochemical GUS assay was performed according to the procedure of Jefferson [33].

Subcellular localization analysis

The full-length cDNA of *ShNPSN11* was cloned into the binary vector pCAMBIA-1302 (harboring GFP label) via *Nco*I restriction enzyme digestion followed by ligation of gene-specific DNA primers (Supplementary Table S2). The resultant expression construct was transformed into *Agrobacterium tumefacien* strain GV3101. *A. tumefaciens* harboring 1302-*ShNPSN11* was cultured in LB broth containing 50 μg/ml, each, of gentamycin, rifampicin, and kanamycin at 28°C, with orbital shaking at 200 rpm. After 24–48 h, the culture was centrifuged at 4000 rpm for 5 min, washed with 10 mM $MgCl_2$ + 10 mM MES (pH 5.6), and suspended to an OD_{600nm} of 0.8 with 10 mM $MgCl_2$ + 10 mM MES (pH 5.6) + 200 μM acetosyringone and incubated at room temperature for 3 h. Leaves of *N. benthamiana* were inoculated with strains containing recombinant plasmid 1302-*ShNPSN11* or the empty vector pCAMBIA-1302. And *A. tumefaciens* harboring PM-RK, a plasma membrane maker with mCherry protein [34], was inoculated, as described above, at the same sites. GFP fluorescence was detected using an Olympus FV1000 laser confocal microscope equipped with a 488 nm filter, and mCherry was detected with TXRED. The experiment was repeated three times.

TRV vectors construction and plant transformation

Plasmid vectors for virus-induced gene silencing (VIGS) were constructed using tobacco rattle virus (TRV1 and TRV2). A 393 bp fragment of *ShNPSN11* containing a *BamHI* restriction enzyme site (Supplementary Table S3) was cloned from the LA1777 cDNA and ligated into the vector pGEM-T Easy (Promega, Madison, WI, U.S.A). Next, the resultant product was ligated into pTRV2 according to the method of Senthil-Kumar et al. [35]. All TRV-based vectors were transformed into *A. tumefaciens* strain GV3101 using the heat shock method [36]. DNA constructs were extracted using the plasmid extraction kit from Tiangen (Shanghai, China) and sequenced to confirm the presence and fidelity of the intended inserts. Cloning of the 425 bp gene fragment of phytoene desaturase (*SlPDS*) (accession number NM_001247166) was performed using the DNA primers listed in Supplementary Table S3. DNA primers were designed using Primer Premier ver. 6.0.

A. tumefaciens carrying pTRV1 and pTRV2, or pTRV2 derivatives, were cultured and infiltrated as previously described by Sun et al. [26]. In brief, 5 ml of an overnight culture was grown at 28°C in the appropriate antibiotic selection medium in a 15 ml glass tube for 24 h, after which the method of harvesting and resuspending *Agrobacterium* cells was same as Senthil-Kumar et al. [37]. Infiltration was performed on the first and second leaves of four-leaf stage LA1777 plants using a 1 : 1 mixture of TRV1 and TRV2-*ShNPSN11*. In parallel, TRV2-expressing *phytoene desaturase* (*PDS*) was used to monitor silencing efficiency. Following virus inoculation, seedlings were transferred to an environmentally controlled growth chamber (25°C, 16 h light/8 h dark photoperiod). Photo-bleaching symptoms in the *PDS* control plants were observed at ~30 days after virus inoculation.

Fungal biomass analyses and quantification of disease severity

For each experiment, two subsets of plants were maintained from each treatment (i.e. TRV2, TRV2-*SlPDS*, or TRV2-*ShNPSN11*). At 7–14 days after inoculation, samples were collected from TRV2 seedlings and TRV2: *ShNPSN11*-silenced seedlings. Total RNA was extracted as described above. Synthesis of complementary DNA (cDNA) was performed using the PrimeScript™ RT Reagent Kit with gDNA Eraser (Takara Biotechnology Co. Ltd., Dalian, China) according to the manufacturer's instructions. Silencing efficiency was evaluated by qRT-PCR using gene-specific primers for *ShNPSN11* (Supplementary Table S4). In parallel to sample for mRNA analysis, samples were collected from 6-time points (6, 12, 24, 48, 72, and 96 hpi) for histological observation. Disease severity was assessed by the former description with 0–9 disease rating scale [38] as mentioned below: 0 = no disease symptoms; 1 = 0–5% of leaves having disease symptoms; 3 = leaves with infection lesions comprising up to 6–10%of the total leaf surface; 5 = leaves with infection lesions up to 11–20% of the total leaf surface; 7 = leaves with infection lesions up to 21–40% of the total leaf surface; and 9 = leaves with infection lesions up to 41–100% of the total leaf surface.

Disease severity indices were calculated using the following equation

$$\text{Disease index (DI)} = \left[\sum(\text{number of diseased plant leaves at a given disease severity} \times \text{the disease severity}) / (\text{total plant leaves analyzed} \times 9)\right] \times 100.$$

An average DI was calculated at three independent time points for each infected plant.

To quantify the accumulation of H_2O_2 (H_2O_2 production rate = H_2O_2 numbers per 100 penetration sites) and the induction of HR cell death (HR production rate = HR numbers per 100 penetration sites) during *On*-Lz infection, the 3,3-diaminobenzidine (DAB; AMERCO, Solon, OH, U.S.A.) staining method [39,40]. In brief, samples collected from 6-time points (6, 12, 24, 48, 72, and 96 hpi) were cut into 2–3 cm^2 segments without the edge and main vein, and then stained as previously described [39,40]. At least 50 penetration sites on each of four-leaf samples were observed at each time point. Standard errors of deviation were calculated using Microsoft Excel. Fungal growth was visualized using trypan blue staining. Leaves were cleared in 100% ethanol, followed by staining in a 0.05% trypan blue solution containing equal parts of water, glycerol and lactic acid. Fungal structures were observed using a dissecting microscope.

Agrobacterium-mediated transient expression in *Nicotiana benthamiana*

A 786 bp fragment of *ShNPSN11* was generated by PCR using gene-specific DNA primers (Supplementary Table S5) and resultant product was cloned into the PVX106 : GFP vector via SalI digestion. The resultant clone was transformed into *A. tumefacien* strain GV3101 according to the method of D'Aoust et al. [41]. Transformants were grown at 28°C in LB media containing 50 μg/ml of each of rifampicin and kanamycin until cultures reached stationary growth. Agrobacterium cultures were centrifuged (5000×***g***) and the resultant bacterial pellets resuspended in infiltration buffer (10 mM $MgCl_2$, 150 μM acetosyringone, 10 mM MES pH 5.6) to a final OD_{600nm} of 0.1. After incubation at room temperature for 2–3 h in the dark, *A. tumefaciens* cells carrying PVX106:*GFP:ShNPSN11* or PVX106:*GFP* were infiltrated into *N. benthamiana*. Buffer alone infiltrations were included as a control. After 24 h, the same infiltration site was challenged with *A. tumefaciens* cells carrying the *BAX* gene, a death-promoting member of the Bcl-2 family of proteins, which triggers cell death when expressed in plants [42]. *A. tumefaciens* strains carrying *GFP* alone was infiltrated into leaves and served as a negative control. Symptom development was evaluated at 5-to-7 days after infiltration. Infiltration experiments were repeated three times, and each assay consisted of three independent leaves from three independent plants.

Data collection and analyses

All experiments were performed in triplicate and at least 50 penetration sites were scored by microscopy at each time point. Statistical analyses were carried out using the IBM SPSS statistics software package (version 20.0). Comparisons between control samples and each treatment were evaluated using a Student's *t*-test at a significance level of $\alpha = 0.05$.

Results

Identification and *in silico* characterization of *ShNPSN11*

Previous work from our group demonstrated a role for SNARE proteins during fungal pathogen infection of wheat [8]. To determine if similar signaling and resistance mechanisms exist in tomato, as well as to interrogate the patterns of differential gene expression of key immune-related mRNAs following *On*-lz infection, we first evaluated a representative set of eight defense- and susceptibility-associated mRNAs for changes in expression following infection. As shown in Figure 1, quantitative real-time PCR (qRT-PCR) analysis revealed a significant induction in *NPSN11* — a gene encoding a member of the tomato SNARE signaling complex — in both the *On*-lz resistant tomato cultivar LA1777, as well as was moderately up-regulated in the susceptible cultivar Money Maker, with a peak in accumulation occurring at 12 hpi. mRNA accumulation of *ShNPSN11* was ~4.8-fold higher in LA1777 than that in Money Maker. In contrast, the mRNA accumulation levels of *SlMEMBER1–1*, *SlSYP61, SlSYP71, SlVAMP721*, and *SlSNAP33* were higher in the susceptible tomato variety Money Maker, indicating that in the resistant LA1777, these genes may not play a significant, induced, role in response to fungal pathogen infection. *NPSN131 and SYP132* were similarly expressed in both LA1777 and Money Maker. Based on these data, we selected *NPSN11* as a candidate SNARE for further analysis.

The open reading frame (ORF) of *ShNPSN11* was determined to be 1524 bp, yielding a predicted protein consisting of 261-amino acid (AA) with a molecular mass of 29.4 kDa. Phylogenetic analysis of ShNPSN11 (Figure 2A), in comparison with additional NPSN11 orthologs, revealed that ShNPSN11 possess a high sequence similarity to *Solanum tuberosum* StNPSN11 (XP_006358624), with an approximate protein identity of 96%. Amino acid sequences alignment of ShNPSN11 with additional SNARE proteins, including AtNPSN11 (NP_565800.1), AtNPSN12 (NP_175258.2), AtNPSN13 (NP_566578.1), OsNPSN11 (AAU94635.1), OsNPSN12 (AAU94636.1), OsNPSN13 (AAU94637.1), TaNPSN11 (AFQ60145.1), TaNPSN12 (AFQ60146.1), and TaNPSN13 (AFQ60147.1), revealed that *ShNPSN11* encodes a protein with a putative C-terminal transmembrane domain (amino acids 212 to 236) and a Qb-SNARE domain at amino acids 142 to 204 (Figure 2B and Supplementary Figure S1). Using ProtComp, a subcellular localization prediction of ‘plasma membrane’ was made for ShNPSN11 (Supplementary Figure S1).

The promoter of *ShNPSN11* was involved in SA and MeJA responsiveness

To gain insight into the expression activity of *ShNPSN1*, a promoter analysis was analyzed by PlantCARE and Softberry. As Figure 3 showed, there were four defence-related motifs in the promoter of *ShNPSN1*: two TGACG-motifs (−215, −365 position), *cis*-acting regulatory element involved in the MeJA-responsiveness; a TCA element (−597 position), *cis*-acting element involved in salicylic acid responsiveness; and a TC-rich repeats (−1392 position), *cis*-acting element involved in defense and stress responsiveness. GUS assays were employed to confirm promoter responsiveness, and as show, we observed that the promoter fusions were responsive to both SA and MeJA treatment. Indeed, following SA or MeJA treatment, GUS activity was highly induced in pCAMBIA0390:: $P_{SlNPSN11}$-GUS, yet was lower in pCAMBIA0390:: 35S-GUS.

ShNPSN11 is localized within the plasma membrane

As noted above, ShNPSN11 is predicted to primarily be localized within the plant plasma membrane. To validate this prediction, a 786 bp fragment of *ShNPSN11* was cloned into the binary expression vector pCAMBIA-1302, transformed into *A. tumefacien* strain GV3101 and transiently expressed in *N. benthamiana*, at the same time, PM-RK also transiently expressed as a maker in the same sites. As shown in Figure 4, at 48 h post-infiltration, 1302-*ShNPSN11* expressed in plasma membrane, because the merged figure of 1302-*ShNPSN11* GFP channel and PM-RK mCherry channel was showed yellow, which implied the proteins of ShNPSN11 and PM-RK was expressed in same location in tobacco cell. While the control inoculation (i.e. pCAMBIA-1302) showed a diffuse localization signal, indicative of non-specific cellular localization, because only the plasma membrane was yellow and others were green. This result was confirming the predicted localization pattern using *in silico* methods.

ShNPSN11 is not required for the activation of a hypersensitive cell death response nor does *ShNPSN11* suppress BAX-induced necrosis

To identify the putative function(s) of ShNPSN11 in plant immunity and defense signaling in response to fungal infection, Agrobacterium-mediated transient expression was used to evaluate *Sh*NPSN11 activity during cell death elicitation in *N. benthamiana*. In short,

infiltrations were conducted using PVX, PVX + BAX, buffer, buffer + BAX, *ShNPSN11*, and *ShNPSN11*+BAX (Figure 5A). As shown in Figure 5B, at 5-days post-injection we did not observe the induction of cell death upon transient expression of PVX, *ShNPSN11*, or buffer alone, indicating that ShNPSN11 does not induce cell death in *N. benthamiana*. However, at 7 days-post-inoculation, obvious necrosis symptoms were visible in leaves infiltrated with Agrobacterium expressing BAX + PVX, BAX + Buffer and BAX + *ShNPSN11* (Figure 5B). Leaves were cleared with a solution of glacial acetic acid and absolute ethanol (1 : 1, volume/volume), and necrosis-associated symptoms were observed (Figure 5C).

ShNPSN11 gene silencing resulted in host susceptibility to *On*-lz

To evaluate the role of *ShNPSN11* during interaction between tomato and *On*-lz, a tobacco rattle virus-induced gene silencing (TRV-VIGS)-based method was used to silence *ShNPSN11* expression in LA1777. TRV2, TRV2: *SlPDS* (*PHYTOENE DESATURASE*), and TRV2:*ShNPSN11* fusion-containing plasmids were inoculated into tomato leaves (Figure 6A) for silencing. To first evaluate the efficacy of the TRV-based approach, TRV2:*SlPDS* was monitored for the induction of photo-bleaching. As shown in Figure 6B, at 4-weeks post-inoculation, a photo-bleaching phenotype was observed, indicating the technical efficiency of TRV-VIGS-mediated gene silencing. In parallel to the analysis of gene silencing efficiency, all TRV-VIGS seedlings were inoculated with *On*-lz and the infection phenotypes were recorded. Compared with control plants (i.e. Figure 6C), plants carrying TRV2:*ShNPSN11* showed obvious powdery mildew disease lesions (Figure 6C–F), with disease indexes values of *ShNPSN11*-silenced plants at significantly higher levels than control plants. Quantification of the degree of silencing efficiency, by qRT-PCR, was shown to be ~64%, indicating a level of silencing consistent with a significant reduction in mRNA accumulation (Figure 6G). Quantification of the disease index, as determined by lesion size indices, in *ShNPSN11*-silenced plants were calculated at 5.8 and 10.0 at 7 and 14 dpi, respectively (Figure 6H). Based on these data, we conclude that *ShNPSN11* is required for resistance to *On*-Lz.

Silencing of *ShNPSN11* reduced defense responses and led to increased growth of *On*-Lz in tomato

To further define how *ShNPSN11* functions in tomato resistance to *On*-Lz, we evaluated the induction of early defense signaling processes, such as the accumulation of H_2O_2 and the induction of the hypersensitive response (HR). In the case of H_2O_2 response signaling, we did not observe the production of reactive oxygen at 6 hpi in either control or *ShNPSN11*-silenced plants (Figure 7A). At 12 hpi, ~3% of the infection sites from control seedlings produced H_2O_2; in *ShNPSN11*-silenced seedlings, the ROS response was observed to be ~4.3%. However, this difference was determined to not be significant (P value = 0.05). At 24 hpi, control seedlings produced more H_2O_2 (30.0%) than *ShNPSN11*-silenced seedlings (~18%), and at 48 hpi, control seedlings maintained an increased number of infection sites producing H_2O_2 (ca. 40.2%), than in *ShNPSN11*-silenced seedlings (ca. 25.4%). This trend continued to increase until ~96 hpi, at which point 41.5% of the infection sites from control plants produced an ROS response, while ~21% of the *NPSN11*-silenced plants generated a ROS response. A similar trend was observed for the induction of the HR revealing an

approximate 20% reduction in pathogen-induced cell death in *NPSN11*-silenced plants at 96 hpi (Figure 7B).

As a second, parallel, microscopic readout for the induction of defense signaling, HR results showed that control plants had more cell death-induced tissue necrosis than was observed in *ShNPSN11*-silenced plants (Figure 7C–H). This data is in agreement with the ROS data, noted above. At 6 hpi (Figure 7C,D), we did not observe the presence of an HR in either the control or *ShNPSN11*-silenced plants. At 12 hpi, although the rate of HR on *ShNPSN11*-silenced seedlings was higher (ca. 4%), than that observed in control plants (ca. 2%), no significant difference was detected (P value = 0.05, Student's t-test). At 48 hpi (Figure 7E,F), the HR in control plants was significantly more pronounced than in *ShNPSN11*-silenced plants (~32% versus ~24%, respectively). At 72 and 96 hpi, the rate of HR induction in control plants was 45.4% and 47%, respectively, which are significantly higher than the rate of *ShNPSN11*-silenced plants (ca. 27% and 28%, respectively) (Figure 7G,H). These data are in agreement with the activation of pathogenesis-related (*PR*) gene expression, whereby we observed that NPSN11 is required for the induced expression (24 hpi) of *PR1b1* (*PR1*), *chitinase 3* (*PR3*), and *thaumatin-like* (*PR5*) gene expression in LA1777 after inoculation with *On*-Lz (Supplementary Figure S2). In total, these data demonstrate that *Sh*NPSN11 plays a role in the rate and/or development of the HR in response to *On*-lz infection.

Lastly, to determine if the observed reduction in defense signaling and resistance responses led to increased fungal growth, we used trypan blue staining to visualize fungal growth in *ShNPSN11*-silenced (Figure 8A,C,E) and control (CK; Figure 8B,D,F) tomato plants over a short time-course of infection. As shown, pathogen growth and colonization were apparent in both control and silenced plants; however, we observed an enhancement in the rate of fungal pathogen development and the overall growth of the pathogen at the end of the time-course. Following inoculation, fungal spore germination was apparent on roots of both hosts, and by 2 days post inoculation (DPI), fungal mycelia had expanded across the root surface. Interestingly, mycelia on corn roots were parallel to root epidermis cells, while mycelia growth on soybean roots did not have any apparent pattern of colonization. Also, by 2 DPI, round and swollen mycelia structures were observed on soybean roots and appear to be similar to penetration structures (e.g. appressoria).

Discussion

The interaction between host and pathogen results in a multitude of cellular and genetic changes, including in both the host and pathogen. Among the best characterized outputs associated with host resistance are the induction of the hypersensitive response (HR), the production of defense-associated metabolites — such as phytoalexin — and rapid changes in protein transport, secretion, and endocytosis [43–46]. In each of these defense-associated processes, vesicle trafficking has been shown to play a key role, and in recent years, a model is emerging whereby membrane fusion processes and the broader function of vesicle trafficking mediate host response to pathogenesis, as well as are actively targeted by pathogens during infection [47].

SNAREs' function and activity vary based on localization and interacting proteins, including to some extent, the cargo transported during trafficking [48–50]. In the case of plant-pathogen interactions, the role of SNAREs has been described [19,51]; however, a detailed inventory of the function and regulation of SNARE-dependent pathogen resistance signaling is lacking. In the current study, we describe the function of *ShNPSN11*, which is required for resistance signaling to the downy mildew pathogen *O. neolycopersici*. In planta expression analysis revealed a potential role for *ShNPSN11* based on the pathogen-induced pattern of mRNA accumulation in resistant tomato (i.e. LA1777). Using this as an initiation point for further analyses, we determined the expression pattern of *ShNPSN11*, including a subset of additional SNARE and defense-associated transcripts, observing that the expression pattern of *ShNPSN11* was similar to previously characterized expression patterns of *TaNPSN11*, a SNARE required for resistance in wheat in response to fungal (*Puccinia striiformis*) infection in wheat [8]. This is not surprising, as our *in silico* analysis demonstrates a high degree of structural/sequence homology to a larger family of SNARE proteins from a wide range of plant species, thus not only demonstrating a conservation in terms of structural similarity, but also a likelihood of conserved functional homology as well. And the promoter analysis found that there were four defence-related motifs in the promoter of *ShNPSN1*: two TGACG-motifs, a TCA element, and a TC-rich repeats. The GUS assay indicated that *ShNPSN11* could response to SA and MeJA stress.

In Arabidopsis, AtNPSN11 was highly expressed in dividing cells, and also was a component of membrane trafficking and fusion machinery in cell plate formation[52]. Based our subcellular localization result, ShNPSN11, as a Qb-SNAREs, was on the target membranes — plasma membrane, which suggested to ShNPSN11 mediate membrane fusion at the plasma membrane.

To confirm the predicted function(s) of *ShNPSN11* during pathogen infection, as well as to investigate the *in planta* activity, we undertook a functional analysis of *NPSN11* using a gene-silencing-based approach (i.e. TRV-mediated gene silencing). Using a TRV-based silencing approach, we identified a role for NPSN11 during resistance signaling following *O. neolycopersici* infection, including in the (downstream) activation of defense-associated signaling processes, including ROS burst signaling and *PR* gene expression. Interestingly, however, and converse to previous evaluation of SNARE function during pathogen infection, we did not observe the induction of, nor suppression of BAX-induced, cell death through ectopic expression of *ShNPSN11*. And while these data, described above, support a role for NPSN11 during immunity, it indicates that *ShNPSN11* is likely not directly responsible for HR induction and/or cell death signaling-associated processes. Indeed, as a function of both ROS and HR signaling activation, silencing of *ShNPSN11* led to a ~20% reduction in both defense-associated outputs, suggesting a possible role for *ShNPSN11* in processes associated with the timing and/or amplitude of the signaling. These data are similar to previously described HR- and ROS-associated genes and their processes [8,53]. Additional evaluation of a comprehensive set of defense-associated genes, and their associated processes, will likely provide the resolution needed to assign a specific function to *ShNPSN11* during fungal pathogen infection.

Supplementary Material

Refer to Web version on PubMed Central for supplementary material.

Acknowledgements

The authors thank Professor Yuejin Wang at Northwest A&F University for providing the pCAMBIA0390-GUS plasmids.

Funding

This work was supported by the Natural Science Foundation of China (grant no. 31571960), Key Industrial Chain Projects of Shaanxi (grant no. 2019ZDLNY03-07) in the laboratory of Q.M. Research in the laboratory of B.D. was supported by the National Institute of General Medical Sciences (1R01GM125743).

Abbreviations

HR	hypersensitive response
LB	Luria–Bertani
MM	Money Maker
ORF	open reading frame
PDS	phytoene desaturase
PM	plasma membrane
PR-1	pathogenesis-related protein-1
SNAREs	N-ethylmaleimide-sensitive factor attachment protein receptors
VIGS	virus-induced gene silencing

References

1. Jones H, Whipps JM and Gurr SJ (2010) The tomato powdery mildew fungus *Oidium neolycopersici*. Mol. Plant Pathol 2, 303–309 10.1046/j.1464-6722.2001.00084.x
2. Lebeda A, Mieslerová B, Petrivalsky N, Luhová L, Špundová M, Sedlárová M et al. (2014) Resistance mechanisms of wild tomato germplasm to infection of *Oidium neolycopersici*. Eur. J. Plant Pathol 138, 569–596 10.1007/s10658-013-0307-3
3. Bai Y, Pavan S, Zheng Z, Zappel NF, Reinstadler A, Lotti C et al. (2008) Naturally occurring broad-spectrum powdery mildew resistance in a central American tomato accession is caused by loss of *MLO* function. Mol. Plant Microbe Interact 21, 30–39 10.1094/MPMI-21-1-0030 [PubMed: 18052880]
4. Lyngkjaer MF, Newton AC, Atzema JL and Baker SJ (2000) The barley *MLO* gene: an important powdery mildew resistance source. J. Agron 20, 745–756 10.1051/agro:2000173
5. Mads Eggert N and Hans TC (2012) Recycling of Arabidopsis plasma membrane PEN1 syntaxin. Plant Signal. Behav 7, 1541–1543 10.4161/psb.22304 [PubMed: 23073012]
6. Schmidt SM, Kuhn H, Micali C, Liller C, Kwaaitaal M and Panstruga R (2014) Interaction of a *Blumeria graminis* f. sp. *hordei* effector candidate with a barley ARF-GAP suggests that host vesicle trafficking is a fungal pathogenicity target. Mol. Plant Pathol 15, 535–549 10.1111/mpp.12110 [PubMed: 24304971]

7. Simone P, Chian K, Natascha C, Ralph P and Paul SL (2008) Activity determinants and functional specialization of Arabidopsis PEN1 syntaxin in innate immunity. J. Biol. Chem 283, 26974–26984 10.1074/jbc.M805236200 [PubMed: 18678865]
8. Wang X, Wang X, Deng L, Chang H, Dubcovsky J, Feng H et al. (2014) Wheat TaNPSN SNARE homologues are involved in vesicle-mediated resistance to stripe rust (*Puccinia striiformis* f. sp. *tritici*). J. Exp. Bot 65, 4807–4820 10.1093/jxb/eru241 [PubMed: 24963004]
9. Antonin W, Holroyd C, Fasshauer D, Pabst S, Mollard GF and Von and Jahn R (2014) A SNARE complex mediating fusion of late endosomes defines conserved properties of SNARE structure and function. EMBO J. 19, 6453–6464 10.1093/emboj/19.23.6453
10. Fukuda R, McNew JA, Weber T, Parlati F, Engel T, Nickel W et al. (2000) Functional architecture of an intracellular membrane t-SNARE. Nature 407, 198–202 10.1038/35025084 [PubMed: 11001059]
11. Noriko I and Takashi U (2014) Membrane trafficking pathways and their roles in plant–microbe interactions. Plant Cell Physiol. 4, 672–686 10.1093/pcp/pcu046
12. Saeed B, Brillada C and Trujillo M (2019) Dissecting the plant exocyst. Curr. Opin. Plant Biol 52, 69–76 10.1016/j.pbi.2019.08.004 [PubMed: 31509792]
13. Salinas-Cornejo J, Madrid-Espinoza J and Ruiz-Lara S (2019) Identification and transcriptional analysis of SNARE vesicle fusion regulators in tomato (*Solanum lycopersicum*) during plant development and a comparative analysis of the response to salt stress with wild relatives. J. Plant Physiol 242, 153018 10.1016/j.jplph.2019.153018 [PubMed: 31472447]
14. Wang P, Sun Y, Pei Y, Li X, Zhang X, Li F et al. (2018) *Gh*SNAP33, a t-SNARE protein from *Gossypium hirsutum*, mediates resistance to *Verticillium dahliae* infection and tolerance to drought stress. Front. Plant Sci 9, 896 10.3389/fpls.2018.00896 [PubMed: 30018623]
15. Yun HS and Kwon C (2017) Vesicle trafficking in plant immunity. Curr. Opin. Plant Biol 40, 34–42 10.1016/j.pbi.2017.07.001 [PubMed: 28735164]
16. Inada N and Ueda T (2014) Membrane trafficking pathways and their roles in plant-microbe interactions. Plant Cell Physiol. 55, 672–686 10.1093/pcp/pcu046 [PubMed: 24616268]
17. Collins NC, Hans TC, Volker L, Stephan B, Erich K, Jin-Long Q et al. (2003) SNARE-protein-mediated disease resistance at the plant cell wall. Nature 425, 973–977 10.1038/nature02076 [PubMed: 14586469]
18. Monika K, Nühse TS, Kim F and Peck S (2007) The syntaxin SYP132 contributes to plant resistance against bacteria and secretion of pathogenesis-related protein 1. Proc. Natl Acad. Sci. U.S.A 104, 11850–11855 10.1073/pnas.0701083104 [PubMed: 17592123]
19. Zhang X, Zhao H, Gao S, Wang WC, Katiyaragarwal S, Huang HD et al. (2011) Arabidopsis argonaute-2 regulates innate immunity via miRNA393-mediated silencing of a Golgi-localized SNARE gene, MEMB12. Mol. Cell 42, 356–366 10.1016/j.molcel.2011.04.010 [PubMed: 21549312]
20. Wei T, Hou X, Sanfaçon H and Wang A (2013) The SNARE protein Syp71 is essential for turnip mosaic virus infection by mediating fusion of virus-induced vesicles with chloroplasts. PLoS Pathog. 9, e1003378 10.1371/journal.ppat.1003378 [PubMed: 23696741]
21. Masayuki F, Tomohiro U, Kazuo E, Yuka N, Takashi U, Akihiko N et al. (2014) Interactomics of Qa-SNARE in *Arabidopsis thaliana*. Plant Cell Physiol. 55, 781–789 10.1093/pcp/pcu038 [PubMed: 24556609]
22. von Mollard GF, Nothwehr SF and Stevens TH (1997) The yeast v-SNARE Vti1p mediates two vesicle transport pathways through interactions with the t-SNAREs Sed5p and Pep12p. J. Cell Biol 137, 1511–1524 10.1083/jcb.137.7.1511 [PubMed: 9199167]
23. Xue M and Zhang B (2002) Do SNARE proteins confer specificity for vesicle fusion? Proc. Natl Acad. Sci. U.S.A 99, 13359–13361 10.1073/pnas.232565999 [PubMed: 12374848]
24. Zhao X, Guo X, Tang X, Zhang H, Wang M, Kong Y et al. (2018) Misregulation of ER-Golgi vesicle transport induces ER stress and affects seed vigor and stress response. Front. Plant Sci 9, 658 10.3389/fpls.2018.00658 [PubMed: 29868102]
25. Sun G, Yang Q, Zhang A, Guo J, Liu X, Wang Y et al. (2018) Synergistic effect of the combined bio-fungicides ε-poly-l-lysine and chitooligosaccharide in controlling grey mould (*Botrytis*

cinerea) in tomatoes. Int. J. Food Microbiol 276, 46–53 10.1016/j.ijfoodmicro.2018.04.006 [PubMed: 29656220]

26. Sun G, Feng C, Guo J, Zhang A, Xu Y, Wang Y et al. (2019) The tomato Arp2/3 complex is required for resistance to the powdery mildew fungus *Oidium neolycopersici*. Plant Cell Environ. 42, 2664–2680 10.1111/pce.13569 [PubMed: 31038756]
27. Zheng Z, Appiano M, Pavan S, Bracuto V, Ricciardi L, Visser RGF et al. (2016) Genome-wide study of the tomato *SlMLO* gene family and its functional characterization in response to the powdery mildew fungus *Oidium neolycopersici*. Front. Plant Sci 7, 380 10.3389/fpls.2016.00380 [PubMed: 27579028]
28. Lin X, Kaul S, Rounsley S, Shea TP, Benito MI, Town CD et al. (1999) Sequence and analysis of chromosome 2 of the plant *Arabidopsis thaliana*. Nature 402, 761–768 10.1038/45471 [PubMed: 10617197]
29. Ma BG, Duan XY, Niu JX, Ma C, Hao QN, Zhang LX et al. (2009) Expression of stilbene synthase gene in transgenic tomato using salicylic acid-inducible Cre/loxP recombination system with self-excision of selectable marker. Biotechnol. Lett 31, 163–169 10.1007/s10529-008-9843-x [PubMed: 18792793]
30. Wang Y, Wang S, Zhao Y, Khan DM, Zheng J and Zhu S (2009) Genetic characterization of a new growth habit mutant in tomato (*Solanum lycopersicum*). Plant Mol. Biol. Rep 27, 431 10.1007/s11105-009-0095-2
31. Schmittgen TD and Livak KJ (2008) Analyzing real-time PCR data by the comparative C(T) method. Nat. Protoc 6, 1101–1108 10.1038/nprot.2008.73
32. Wang L, Xie X, Yao W, Wang J, Ma F, Wang C et al. (2017) RING-H2-type E3 gene VpRH2 from Vitis pseudoreticulata improves resistance to powdery mildew by interacting with VpGRP2A. J. Exp. Bot 7, 1669 10.1093/jxb/erx033
33. Jefferson RA (1987) Assaying chimeric genes in plants: the GUS gene fusion system. Plant Mol. Biol. Rep 5, 387–405 10.1007/BF02667740
34. Nelson BK, Cai X and Nebenführ A (2010) A multicolored set of in vivo organelle markers for co-localization studies in Arabidopsis and other plants. Plant J. 51, 1126–1136 10.1111/j.1365-313X.2007.03212.x
35. Senthil-Kumar M, Hema R, Anand A, Kang L, Udayakumar M and Mysore K (2007) A systematic study to determine the extent of gene silencing in *Nicotiana benthamiana* and other Solanaceae species when heterologous gene sequences are used for virus-induced gene silencing. New Phytol. 176, 782–791 10.1111/j.1469-8137.2007.02225.x [PubMed: 17997764]
36. Weigel D and Glazebrook J (2006) Transformation of Agrobacterium using the freeze-thaw method. CSH Protoc. 2006, 1031–1036 10.1101/pdb.prot4666
37. Senthil-Kumar M, Govind G, Kang L, Mysore KS and Udayakumar M (2007) Functional characterization of *Nicotiana benthamiana* homologs of peanut water deficit-induced genes by virus-induced gene silencing. Planta 225, 523–539 10.1007/s00425-006-0367-0 [PubMed: 16924536]
38. Correll JC, Gordon TR and Elliot VJ (1988) Powdery mildew of tomato: the effect of planting date and triadimefon on disease onset, progress, incidence, and severity. Phytopathol 78, 512–519 10.1094/Phyto-78-512
39. Wang J, Hai Z, Yan H, Feng C, Yang W and Ma Q (2015) Evaluation of actin cytoskeleton in non-host resistance of pepper to *Puccinia striiformis* f. sp. *tritici* stress. Physiol. Mol. Plant Pathol 92, 112–118 10.1016/j.pmpp.2015.09.003
40. Wang J, Wang Y, Liu X, Xu Y and Ma Q (2016) Microtubule polymerization functions in hypersensitive response and accumulation of H2O2 in wheat induced by the stripe rust. Biomed. Res. Int 2016, 7830768 10.1155/2016/7830768 [PubMed: 27610380]
41. D'Aoust MA, Lavoie PO, Couture MM, Trépanier S, Guay JM, Dargis M et al. (2010) Influenza virus-like particles produced by transient expression in *nicotiana benthamiana* induce a protective immune response against a lethal viral challenge in mice. Plant Biotechnol. J 6, 930–940 10.1111/j.1467-7652.2008.00384.x

42. Lacomme C and Santa C (1999) Bax-induced cell death in tobacco similar to the hypersensitive response. Proc. Natl Acad. Sci. U.S.A 96, 7956–7961 10.1073/pnas.96.14.7956 [PubMed: 10393929]
43. Eggert D, Naumann M, Reimer R and Voigt CA (2014) Nanoscale glucan polymer network causes pathogen resistance. Sci. Rep 4, 4159 10.1038/srep04159 [PubMed: 24561766]
44. Mendes-Giannini MJ, Soares CP, da Silva JL and Andreotti PF (2010) Interaction of pathogenic fungi with host cells: Molecular and cellular approaches. FEMS Immunol. Med. Microbiol 45, 383–394 10.1016/j.femsim.2005.05.014
45. Thordal-Christensen H, Zhang Z, Wei Y and Collinge D (2010) Subcellular localization of H_2O_2 in plants. H_2O_2 accumulation in papillae and hypersensitive response during the barley—powdery mildew interaction. Plant J. 11, 1187–1194 10.1046/j.1365-313X.1997.11061187.x
46. Yang Y, Shah J and Klessig DF (1997) Signal perception and transduction in plant defense responses. Gene Dev. 11, 1621–1639 10.1101/gad.11.13.1621 [PubMed: 9224713]
47. Sanderfoot AA, Kovaleva V, Zheng H and Raikhel NV (1999) The t-SNARE AtVAM3p resides on the prevacuolar compartment in Arabidopsis root cells. Plant Physiol. 121, 929–938 10.1104/pp.121.3.929 [PubMed: 10557242]
48. Saito C and Ueda T (2009) Functions of RAB and SNARE proteins in plant life. Int. Rev. Cell Mol. Biol 274, 183 10.1016/S1937-6448(08)02004-2 [PubMed: 19349038]
49. Surpin M, Zheng H, Morita MT, Saito C, Avila E, Blakeslee JJ et al. (2003) The VTI family of SNARE proteins is necessary for plant viability and mediates different protein transport pathways. Plant Cell 15, 2885–2899 10.1105/tpc.016121 [PubMed: 14615598]
50. Uemura T, Kim H, Saito C, Ebine K, Ueda T, Schulzelefert P et al. (2012) Qa-SNAREs localized to the trans-Golgi network regulate multiple transport pathways and extracellular disease resistance in plants. Proc. Natl Acad. Sci. U.S.A 109, 1784–1789 10.1073/pnas.1115146109 [PubMed: 22307646]
51. Johansson ON, Fantozzi E, Fahlberg P, Nilsson AK, Buhot N, Tor M et al. (2014) Role of the penetration-resistance genes PEN1, PEN2 and PEN3 in the hypersensitive response and race-specific resistance in *Arabidopsis thaliana*. Plant J. 79, 466–476 10.1111/tpj.12571 [PubMed: 24889055]
52. Zheng H, Bednarek SY, Sanderfoot AA, Alonso J, Ecker JR and Raikhel NV (2002) NPSN11 is a cell plate-associated SNARE protein that interacts with the syntaxin KNOLLE. Plant Physiol. 129, 530–539 10.1104/pp.003970 [PubMed: 12068098]
53. Bao YM, Wang JF, Huang J and Zhang HS (2008) Cloning and characterization of three genes encoding Qb-SNARE proteins in rice. J. Mol. Gen 279, 291–301 10.1007/s00438-007-0313-2

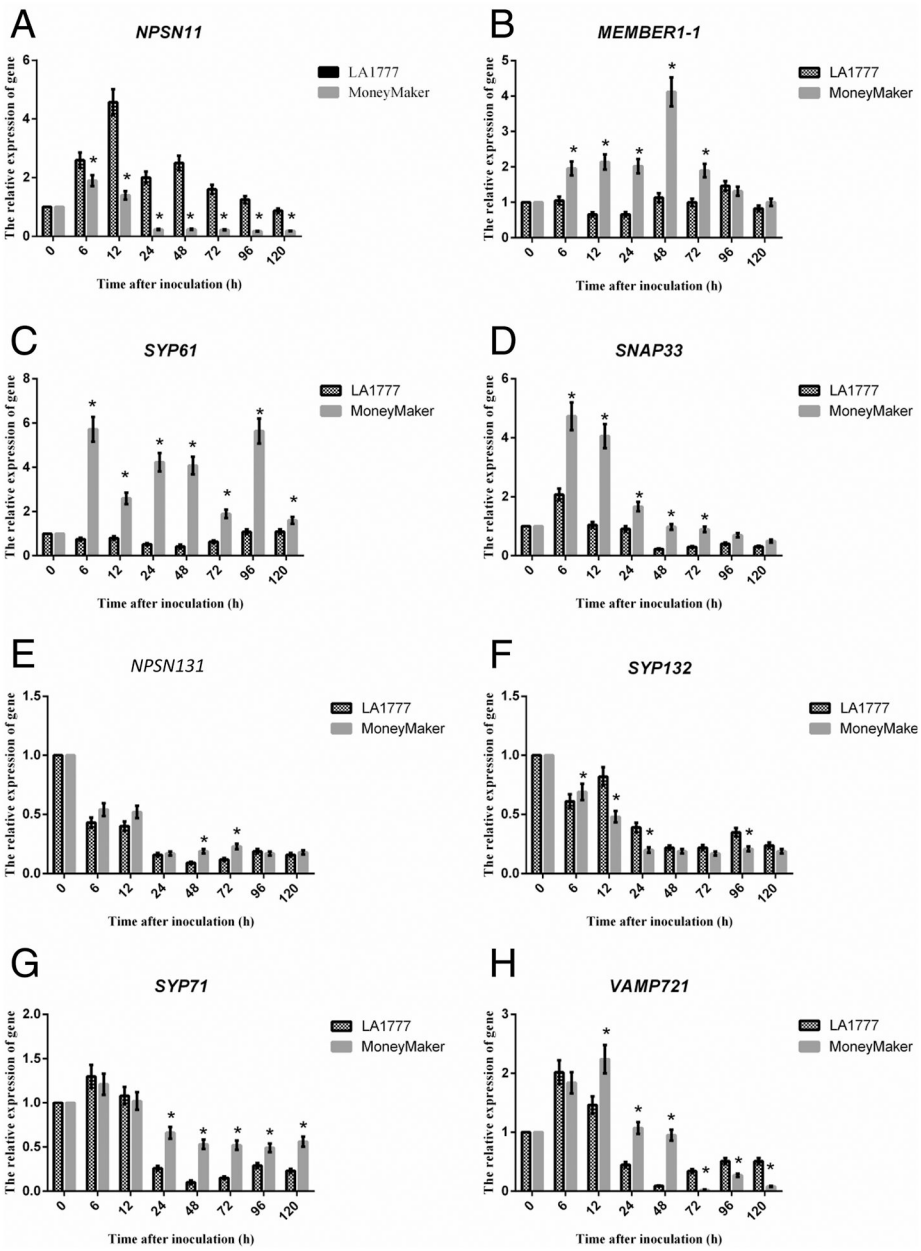

Figure 1. mRNA accumulation of SNARE and vesicle trafficking associated transcripts following *On*-lz infection of resistant and susceptible tomato varieties.

Quantitative real-time PCR (qRT-PCR) analysis of mRNA accumulation of SNAREs genes. (A) *NPSN11* was significantly up-regulated in resistant LA1777 than susceptible cultivar Money Maker. In contrast, (B) *MEMBER1–1*, (C) *SYP61*, and (D) *SNAP33* were significantly up-regulated in susceptible cultivar Money Maker than resistant LA1777. Meanwhile, (E) *NPSN13*, (F) *SYP132*, (G) *SYP71*, and (H) *VAMP721* were also significantly up-regulated in susceptible cultivar Money Maker than resistant LA1777 at the end of the test time. For mRNA expression analyses, 4-week-old LA1777 (resistant) and Money Maker (susceptible) tomato plants (leaves) were spray inoculated with *On*-lz (~10^5 spores ml^{-1}) and incubated at 22°C for up to 5 days. For analysis of mRNA accumulation

following pathogen infection, samples were collected at the indicated time points (time after-inoculation (h)). Total RNA was extracted from leaves and one microgram of total RNA was used for first-strand cDNA synthesis. All DNA primers used for quantitative real-time PCR (qPCR) are listed in Supplementary Table S1. *GLYCERALDEHYDE-3-PHOSPHATE DEHYDROGENASE* (*SlGAPDH*) was used as an internal control for amplification. Expression values are represented as mean ± standard error of the mean (SEM). Statistical analysis was evaluated using a two-way ANOVA, followed by the Bonferroni post-test as compared with time 0. P values ≤0.05 were considered significant, where * $P < 0.05$.

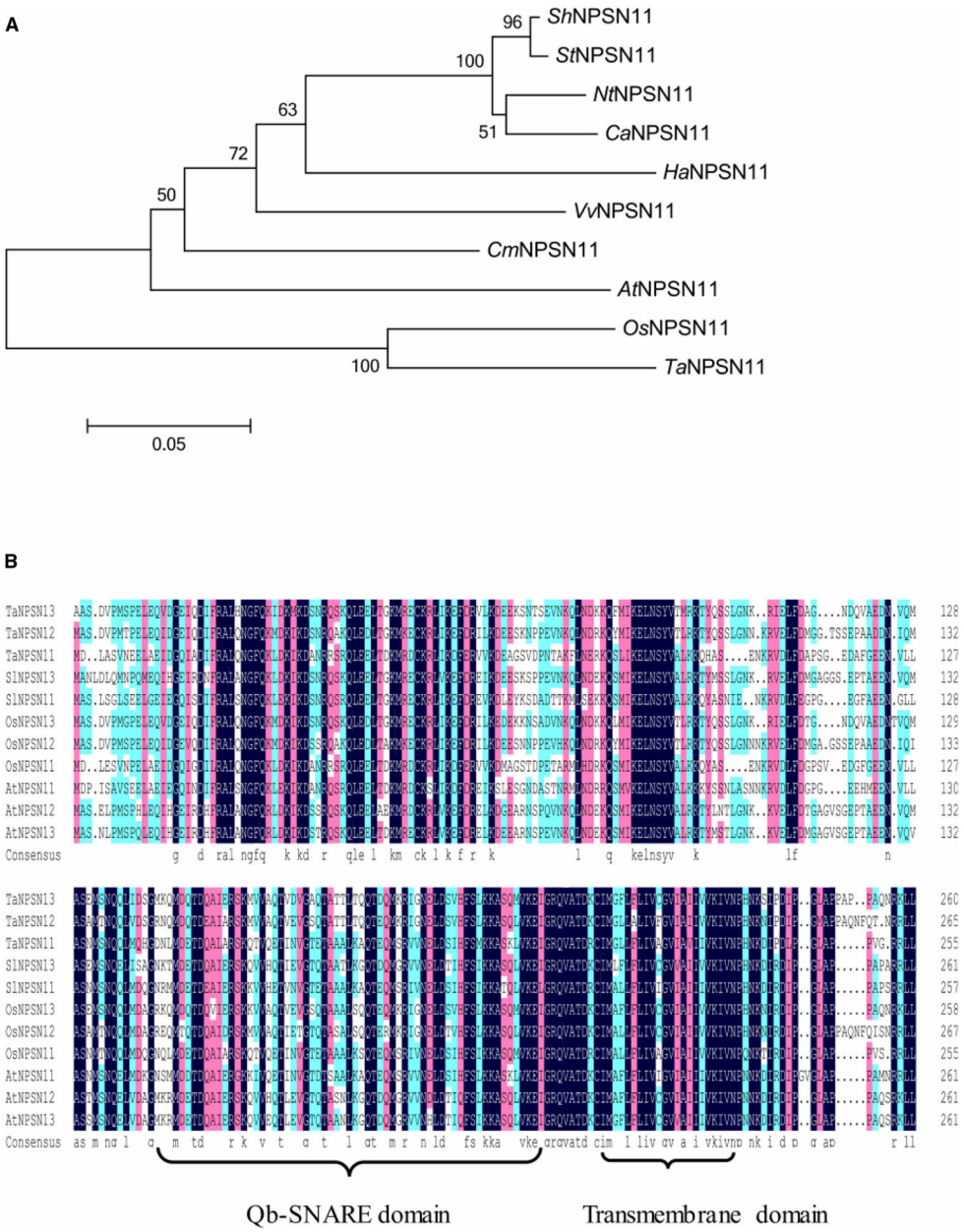

Figure 2. Phylogenetic analysis of ShNPSN1 reveals similarity to known SNARE proteins.

(**A**) Phylogenetic analysis of ShNPSN11, in comparison with AtNPSN11 (NP_565800), OsNPSN11 (AAU94635), TaNPSN11 (AFQ60145), NtNPSN11 (XP_016570058.1), StNPSN11 (XP_006358624), CaNPSN11 (XP_016571158.1), VvNPSN11 (CAN77481), HaNPSN11 (XP_022020789), and CmNPSN11 (XP_008448761), revealed that ShNPSN11 possess a high sequence similarity to *Solanum tuberosum* StNPSN11 (XP_006358624), with an approximate protein identity of 96%. (**B**) Amino acid sequences alignment of ShNPSN11 with AtNPSN11 (NP_565800.1), AtNPSN12 (NP_175258.2), AtNPSN13 (NP_566578.1), OsNPSN11 (AAU94635.1), OsNPSN12 (AAU94636.1), OsNPSN13 (AAU94637.1), TaNPSN11 (AFQ60145.1), TaNPSN12 (AFQ60146.1), and TaNPSN13 (AFQ60147.1). A

predicted C-terminal transmembrane domain (aa 214 to 234) and a Qb-SNARE domain (aa 142 to 204) in ShNPSN11 is shown.

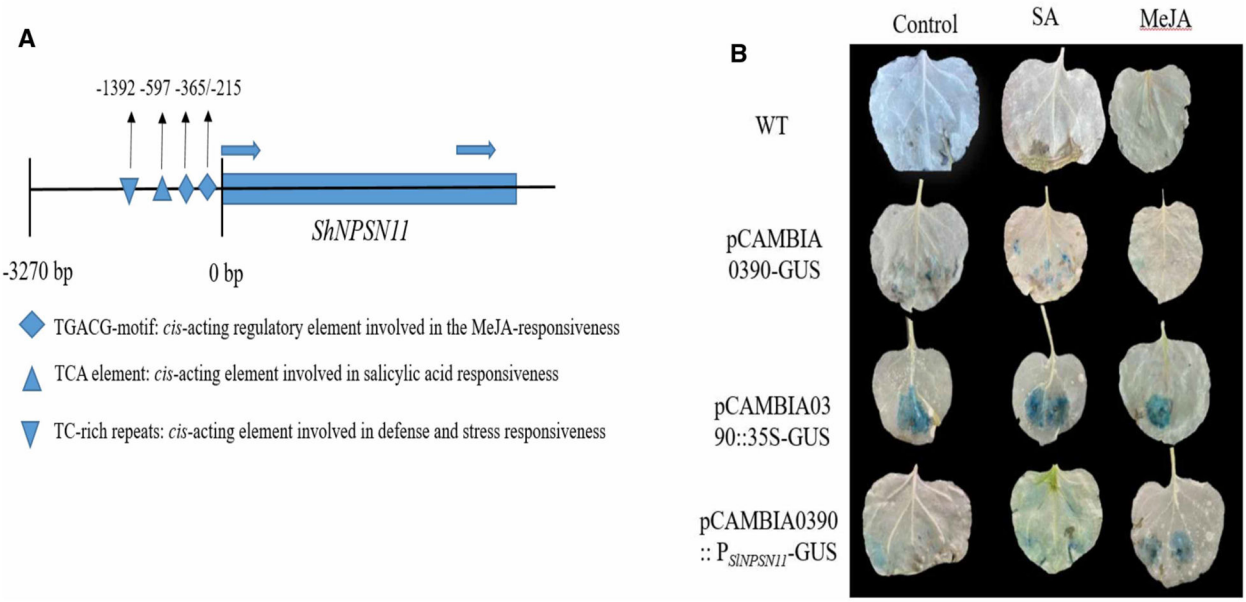

Figure 3. The promoter of *ShNPSN11* are response to SA and MeJA.

(**A**) A *silico* analysis found there four defence-related motifs in promoter of *ShNPSN11*, containing two TGACG-motifs (−215, −365 position), TCA element (−597 position), and a TC-rich repeats. (**B**) Histochemical GUS assay was performed in the transient expression *N. benthamiana*, which were cultivated in a 22°C chamber with 16 h light/8 h dark cycle for 2 days before the treatment with 100 μM MeJA, mM SA and water (CK) (Sigma, Shanghai, China), respectively.

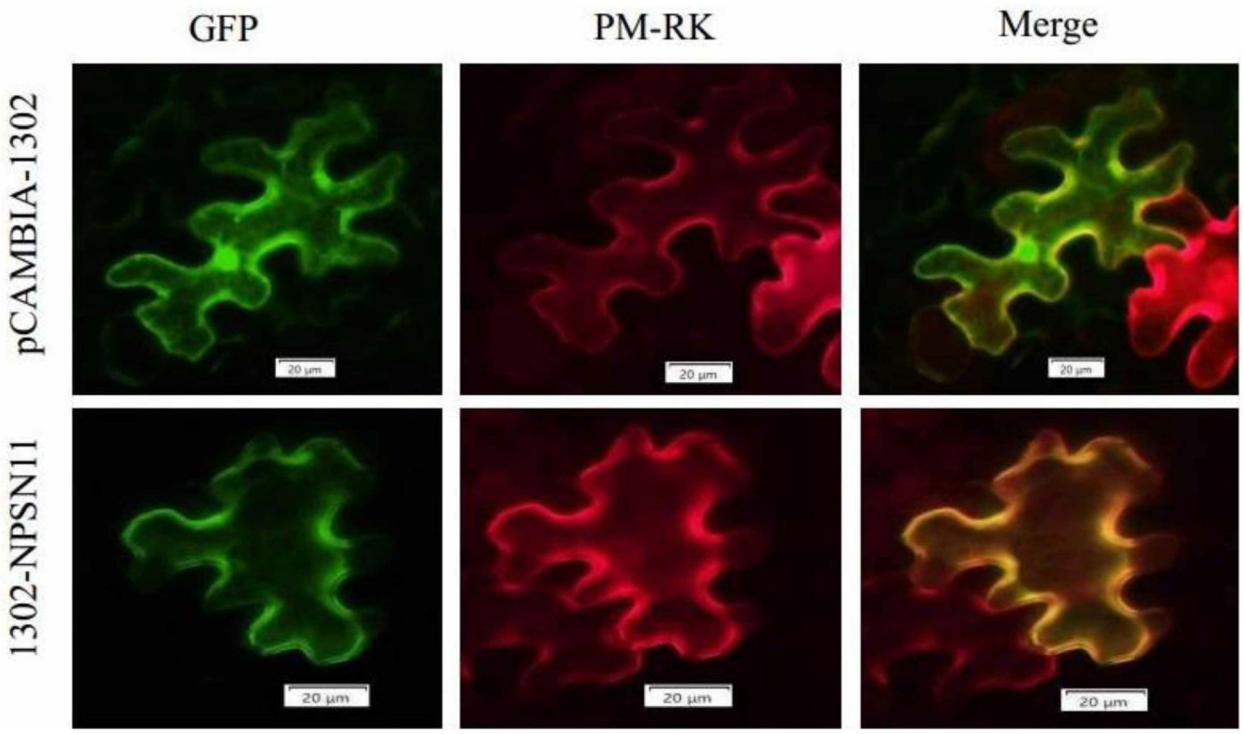

Figure 4. ShNPSN11 is localized in the plasma membrane.

Using Agrobacterium-mediated transient expression, 1302-ShNPSN11 and pCAMBIA1302 (vector control, GFP only) was transiently expressed in tobacco cells. ShNPSN11 was expressed as a C-terminal GFP fusion protein. Images were collected by laser confocal scanning microscopy at 24 h post-inoculation. GFP, fluorescent signal at 488 nm. Chlorophyll signal is shown to indicate autofluorescence of plant tissue. Merge indicates 'overlay' of the GFP and chlorophyll channels.

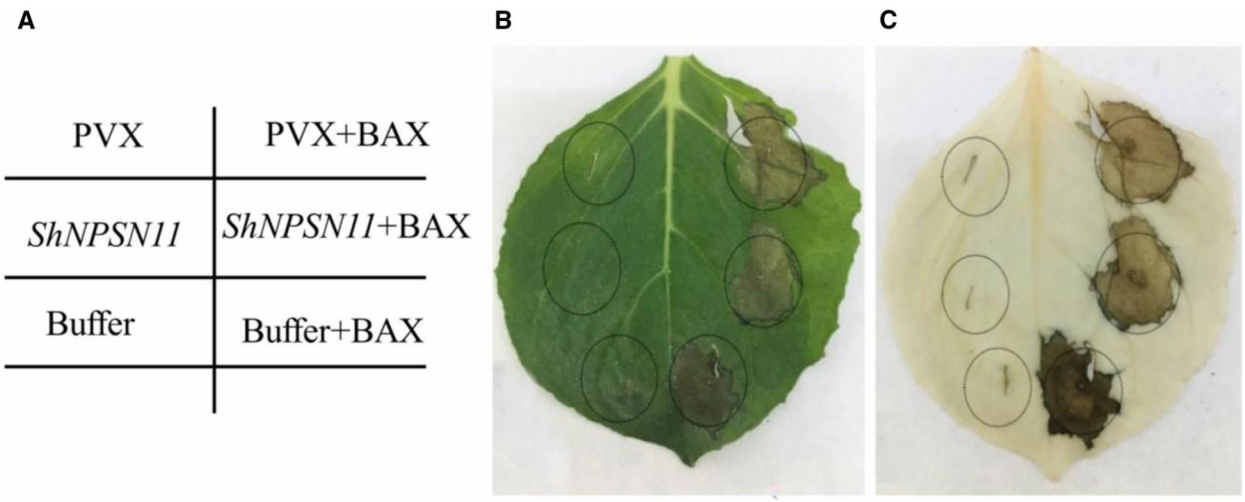

Figure 5. Tobacco transient expression of *ShNPSN11* gene results.

(**A**) Agrobacterium infection tobacco injection diagram. (**B**) Transient expression of *ShNPSN11* does not induce cell death/necrosis, nor does expression block BAX-induced cell death. (**C**) Ethanol and glacial acetic acid (1 : 1) clearing of leaf tissue for enhanced visualization of cell necrosis.

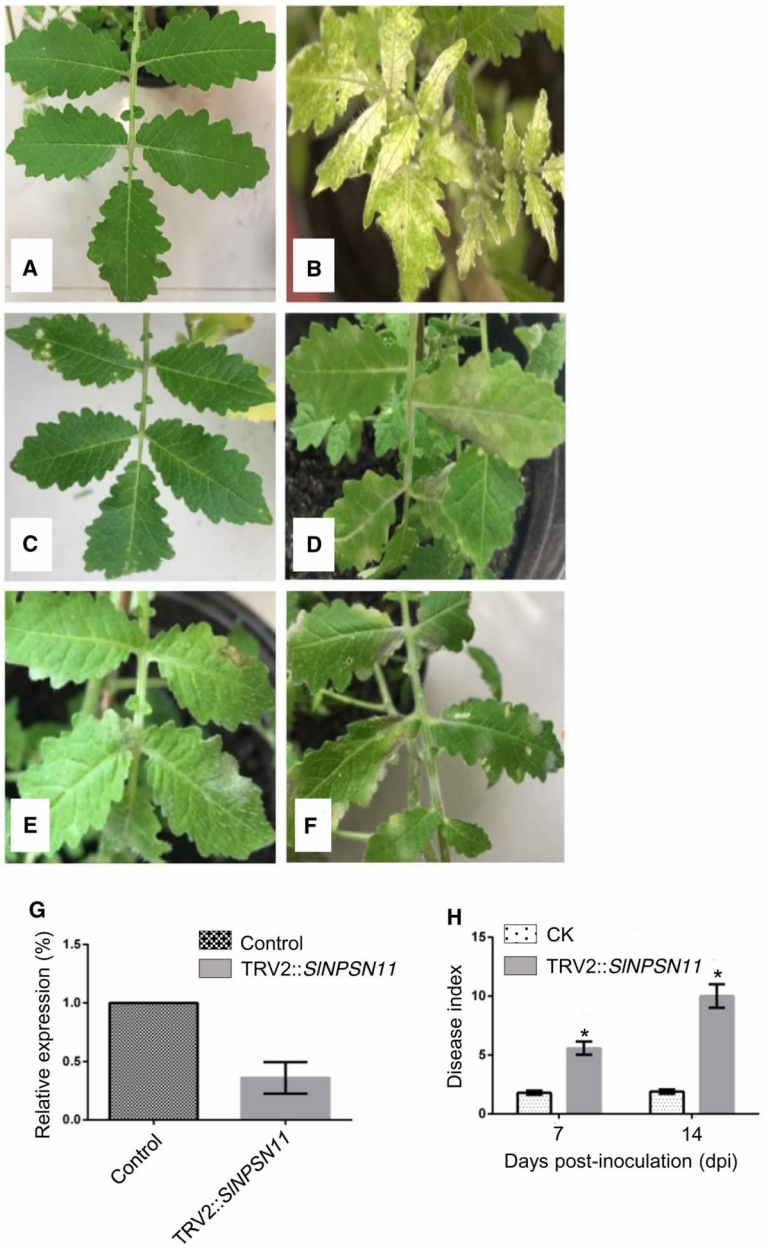

Figure 6. TRV-based silencing of *ShNPSN11* leads to enhanced susceptibility to On-lz.

(**A**) Phenotypes of TRV2 (CK; control) expression in LA1777. (**B**) Phenotype of TRV2:*SlPDS* expression in LA1777. (**C**) LA1777 + TRV2 (control) silenced plant 7-days-post-inoculation with *On*-lz. (**D**) LA1777 + TRV2:*ShNPSN11*-silenced plant 7-days-post-inoculation with *On*-lz. (**E**) LA1777 + TRV2 (control) silenced plant 14-days-post-inoculation with *On*-lz. (**F**) LA1777 + TRV2:*ShNPSN11*-silenced plant 14-days-post-inoculation with *On*-lz. (**G**) Real-time PCR quantification of *ShNPSN11* mRNA accumulation, post-silencing, at 14-days-post-inoculation with control (TRV2) and TRV2:*ShNPSN11*. (**H**) Quantification of disease in LA1777 + TRV2:*ShNPSN11*-silenced plants at 7- and 14-days-post-inoculation with *On*-lz. The asterisk indicates statistically significant differences in disease index between untreated (CK) and TRV2 plants.

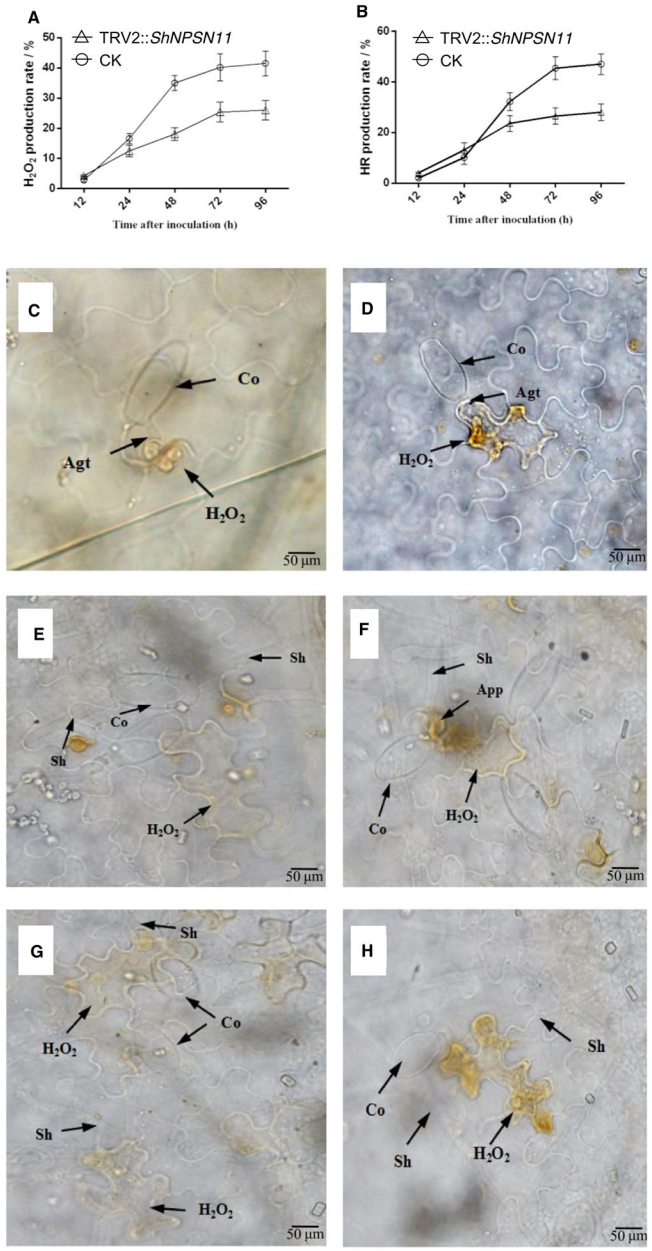

Figure 7. The expression of *ShNPSN11* and disease index in *ShNPSN11*-silenced plant.

(**A**) HR production rate of tomato leaves carrying TRV2 (CK) or TRV2:*ShARPC3* at 6, 18, 24, 48, and 72 hpi, respectively. (**B**) H_2O_2 production in CK or TRV2:*ShARPC3* tomato leaves at 6, 18, 24, 48, and 72 hpi, respectively. (**C–H**) Microscopic detection of H_2O_2 accumulation at interaction sites of *O. neolycopersici* with control (**B**,**D**,**F**) and silenced ShNPSN11 (**A**,**C**,**E**). Co, conidium; App, appressorium; Agt, appressorium germ tube; Sh, secondary hyphae. Bar, 50 μm.

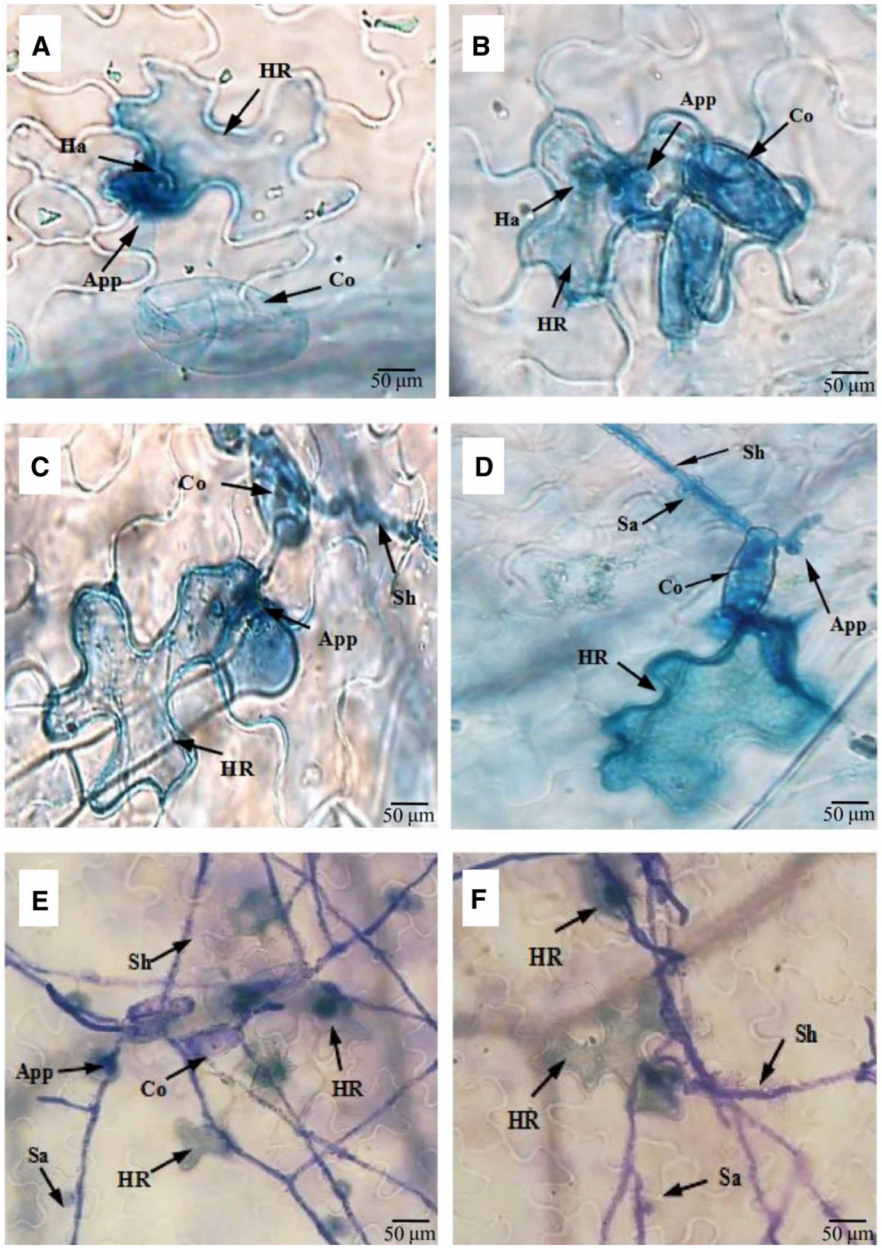

Figure 8. Silencing of *ShNPSN11* leads to increased growth of *O. neolycopersici*.

Microscopic detection of HR accumulation at interaction sites of *O. neolycopersici*. Trypan blue staining of silenced *ShNPSN11* (**A**,**C**, and **E**) and control (**B**, **D**, and **F**) plants following infection with *On*-lz. Co, conidium; App, appressorium; Ha, haustorium; Sh, secondary hyphae; Sa, secondary appressorium; HR, hypersensitive response. Bar, 50 μm.